Effect of solar radiation and humidity on the inner core of walls in historic buildings

M.I. Martínez-Garrido* [a,b], S. Aparicio [c], R. Fort [a,b], J.J. Anaya [c], M.A.G. Izquierdo [b,d]

[a] Instituto de Geociencias, IGEO, (CSIC-UCM), C/José Antonio Novais, 2, 28040 Madrid, Spain
[b] CEI Campus Moncloa, UCM-UPM and CSIC, Madrid, Spain
[c] Instituto de Tecnologías Físicas y de la Información ''Leonardo Torres Quevedo'' ITEFI (CSIC), Arganda del Rey, 28500 Madrid, Spain
[d] E.T.S.I. Telecomunicación (UPM), Av. Complutense # 30, 28040 Madrid, Spain

abstract

The structure of historic buildings and the materials used in their construction, along with outdoor con- ditions, affect indoor temperature and humidity. The walls of San Juan Bautista Church at Talamanca de Jarama, Madrid, Spain, exhibit differences in water absorption, whose explanation is to be found in the various types of construction involved in its over seven centuries of building history, the weather condi- tions and the walls orientation. The south wall fluctuations in inner temperature and humidity produce 11–16 h thermal lag and a very low decrement factor ensuring comfortable interiors all year round with minimal fluctuations in temperature.

1. Introduction

The climate to which a building material is exposed has a very direct effect on its indoor temperature and humidity, which can be controlled by the wall structure [1–3]. Temperature and humidity distributions vary with building and wall orientation, while solar radiation, wind and rain affect not only wall surfaces but their inner cores as well.

The impact of outdoor conditions on the inner wall and on the indoor temperature and humidity of different rooms is more complex in heritage buildings, which throughout their service life often undergo a number of restorations involving different building materials and construction techniques [4]. Moreover, heritage buildings exhibit wide architectural variability due to the long construction times involved, often measured in decades or even centuries in the case of cathedrals. Such variability can be attributed to factors such as changes in works supervision, the depletion of the initial quarries, alterations the initial design for technical or aesthetic reasons or complete overhauls of architectural style [5].

Such buildings are generally also the object of enlargements or rehabilitations to repair damage due to earthquakes, fire or acts of war. The effects of climate on a building's structure can hardly be understood without a knowledge of its construction history. Diligent assessment also includes a study of the building's urban surrounds and how they have changed since it was built, including factors such as the presence of adjacent buildings or trees or the type of outside pavement, which can affect the degree of solar radiation and the impact of rain and wind on wall surfaces.

Moisture, one of the agents of decay in historic buildings, is transferred to their structure primarily by capillary absorption, condensation, rainwater infiltration or leaking pipes. The causes of material decay can be gleaned from information on variations in temperature and humidity [6], which favour chemical decay through dissolution and oxidation, physical decay via salt crystallisation [7,8] or biodeterioration in the form of microbial colonisation [9,10]. Once the microclimatic conditions prevailing in walls are determined, the causes of decay can be established and guidelines defined for their restoration and conservation [11–13].

Moisture in building façades shortens the durability of their materials and raises maintenance costs. It also affects indoor insulation from the elements, to the detriment of environmental control system performance and consequently energy savings [14].

Moreover, wall construction systems affect indoor environmental conditions and comfort levels: a single layer of a homogeneous material performs very differently in this respect from multiple layers of different materials with different thicknesses and thermo-hydraulic properties [13,15–18].

The variations expected in weather conditions in the decades to come due to climate change will induce significant decay in buildings [19,20]. In the region of Madrid, the high temperature is expected to rise by 3–4 by 2060, while precipitation is estimated to decline by 2–20% [21].

Monitoring the parameters to be studied is one of the imperatives microclimatic research [22,23]. Sensors must be positioned to favour continuous data collection not only inside and outside the building, but inside the walls themselves.

The present study aimed to establish the impact of outdoor conditions on the temperature and humidity inside the walls of a twelfth century building, instrumented with a network of wireless sensors.

2. Church construction

San Juan Bautista Church at Talamanca de Jarama, Madrid, Spain (W3 30′54.0″, N40 44′46.0″), a building with a historic-artistic monument listing since 3 June 1931, was chosen to study the effects of climate on the inner cores of walls. The church is sited at an elevation of 655 m above sea level in a rural environment with a Mediterranean climate. The mean annual temperature is 14 C and the area's 445-mm yearly rainfall is recorded primarily in spring and autumn.

This twelfth–thirteenth century Romanesque building originally consisted of a single nave headed by a stone apse, which is all that presently remains of that initial structure. The central nave was demolished in the sixteenth century to enlarge the temple, which was rebuilt in Renaissance style. The new central nave is connected to two side naves by wide span basket arches resting on sturdy columns whose flowery capitals also support a Mudéjar style wooden ceiling [24]. The Baroque bell tower was built later, between the seventeenth and eighteenth centuries. By the nineteenth century, the south façade and bell tower of the church was severely damaged by time and the elements. On the occasion of its reconstruction beginning in 1885, the nave was widened.

The church now measures 36.50 12.70 10.50 m. The walls are 50 cm thick in the nave, 60 cm in the apse and 100 cm in the proximity of the bell tower.

The church lies at 40–50 cm below street level. It is sited in a square with ample space around its main façade, which faces west and south. No trees or other elements outside the building presently alter the solar radiation to which these façades are exposed. Nonetheless, two structures on the building itself cast shadows on the south façade: the tower and the portico at the entrance on that side of the church.

The church apse and its two entrance portals are made of locally quarried dolostone ashlars [25] (Fig. 1a). The indoor columns are also made of this material.

The variation in the façade masonry mirrors the changes in construction techniques over time. The north façade is characterised by bonded brick corners and panes of rubble masonry comprising large rough-hewn siliceous stone bordered by courses of brick. It rests on a 53-cm high rubble stone dado made of similar material and rendered on the inside with clay mortar (Fig. 1b). On the more carefully designed south façade, the fill consists mostly of limestone rubble separated horizontally by two rows of brick (Fig. 1c), although a few quartzite and even an occasional granite stone are also visible, along with Visigoth adornments. The whole wall rests on an 80–90-cm high limestone ashlar dado. This façade has three large inwardly tapered windows. The rubble masonry dado in this wall must have been added as a cladding for the interior brick dado.

The main, eastward facing portal has ashlar stone quoins bonded to the north and south walls, an 85-cm high limestone ashlar dado and a rubble masonry wall alternating with a few rows of brick. The portal is adorned with a semicircular arch and a triangular pediment with Renaissance-type Tuscan columns. The south portal, positioned close to the church tower, is protected by a canopy roof resting on two columns (Fig. 1a).

The church inside walls are rendered with a 5–7-cm layer of cement, in turn surfaced with several coats of plaster and paint. This indoor surfacing has been damaged by capillary water to a height

Fig. 1. San Juan Bautista Church at Talamanca de Jarama. (a) South façade showing the church apse and south entrance canopy; (b) north façade; (c) west façade; (d) stone dado and brick and rubble stone checkerboard arrangement on the south façade; (e) rubble stone dado and wall on the north façade; (f) ashlar stone dado on the west façade and rubble stone masonry on the south façade.

of 1.5 m. Salt efflorescence, a cause of segregation, is visible on the stone surface in the apse [26].

3. Methodology

Monitoring and data gathering were performed with two networks of wireless sensors: one that recorded the outdoor weather conditions (meteo station, Fig. 2a) and the other the humidity and temperature inside the church walls. The monitoring system for monitoring outdoor conditions was fitted with Libelium [27] relative humidity and temperature sensors, as well as an anemometer, rain gauge and wind vane. The in-wall conditions were monitored with MEMSIC instruments [28]. In-wall sensors were embedded at five monitoring points or motes, whose positions were determined based on the degree of decay identified and wall orientation.

The monitoring point numbering reflects the positions finally determined after ruling out sites found to be unsuitable or where anomalous mote operation was identified. The motes were fitted with Sensirion SHT11 sensors to record the temperature and humidity inside and outside the wall and then convey the information to a database node. Sensirion SHT11 sensors, which operate at 0–100% relative humidity with an accuracy of ±3.0% and at temperatures of 40 to +125 C with ±0.4 C accuracy, have built-in signal processing elements with a very small footprint and deliver automatically calibrated and digitised readings [29]. The wireless network that monitored conditions inside the walls comprised sensors positioned at depths, measured from inside the church, of 20 cm (motes 2, 4, 6 and 7) or 10 cm in the apse (mote 1). They were placed at heights of 40, 140 and 240 cm from the indoor flooring (Fig. 2b). The indoor temperature and relative humidity, in turn, were monitored at heights of 40 and 240 cm, with 1-wire/iButton sensors that operated at 0–100% relative humidity with an accuracy of ±5.0% and at temperatures of 20 to +85 C with an accuracy of ±0.5 C.

Conditions were monitored from 1 December 2011 to 30 November 2012. The indoor and in-wall temperature and relative humidity motes (MEMSIC technology) recorded data every 2 min and transmitted the information to a base station (Fig. 2a) where they were collected and processed. This station was connected to a laptop computer fitted graphic processing tools and interfaces developed to interpret the data, as well as an internet connection for remote control. The Libelium technology base station, which received the data recorded at the meteo station every 5 min, was also connected to this computer.

4. Results

4.1. Climate in building surrounds

Talamanca de Jarama has a semi-arid continental Mediterranean climate, with very hot dry summers (highest temperature recorded in the period studied, 41.6 C) and very cold winters, with below freezing temperatures (lowest temperature recorded in the period studied, 5.4 C). The total yearly rainfall varies widely, but is heaviest in April, October and November. The mean relative humidity recorded was 57.1%, although it fluctuated widely, with values of over 90% in rainy periods. The prevailing winds blow from the west and northwest, contributing to the differences observed among the façades. The highest summer solstice-related temperature, recorded in June, was 19.26 C higher than the monthly mean. Smaller temperature differences were recorded in winter, when the highest winter solstice-related temperature recorded was 11.7 C higher than the mean value for that month.

The mean yearly indoor temperature was 3.7 C higher than the outdoor mean and the relative humidity was 11.3% lower. In the winter, the indoor temperatures were milder than the outdoor mercury, particularly when the latter dipped to below freezing. The indoor temperature ranged more widely in the summer than in the winter.

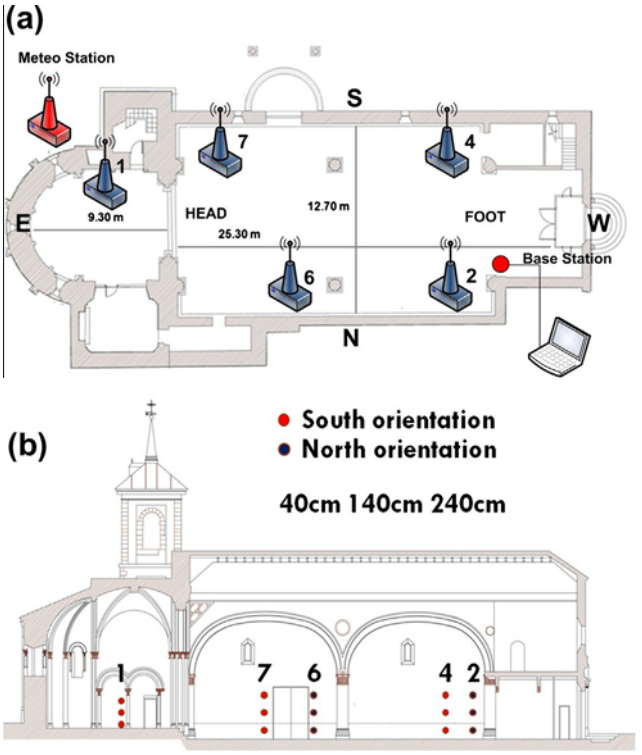

Fig. 2. (a) Plan view of motes used to measure indoor (blue, MEMSIC technology) and outdoor (red, Libelium technology) conditions; (b) height of MEMSIC RH/T motes. (For interpretation of the references to colour in this figure legend, the reader is referred to the web version of this article.)

4.2. Temperature and humidity in walls

4.2.1. Effect of humidity

The church walls had a very high humidity: the sensors located at 40 cm off the floor on both the north and south walls were consistently saturated, with humidity readings of 95–100%. The sensors positioned at 140 cm were likewise saturated throughout the year, with the exceptions of mote 1 on the ashlar stone apse wall, where the highest values hovered around 60–64%, and mote 7 near the south entrance, where the highest humidity ranged from 60% to 62% (Fig. 3). Both these latter sensors detected lower humidity in the summer, with a steady decline from 64% to 57% in the apse and from 62% to 60% in the south wall. The readings delivered by these sensors tended to rise in autumn and winter (Fig. 3).

The widest fluctuations in temperature and relative humidity were recorded by the sensors at a height of 240 cm on the walls most heavily impacted by weather conditions. Fig. 4 shows the coldest (a) and warmest (b) periods recorded by the 240-cm high sensors at each mote.

At that height, in-wall humidity was greatest in the north wall, and in particular at the foot of the church (mote 2), where values ranged from 72–77% in winter to 60–68% in the summer. The lowest RH values were recorded in July and August. Similar readings were found at the head (apse or east side) of the church in the north wall (mote 6, see Fig. 4), although the relative humidity was lower in the winter as well as in the summer, when the means ranged from 55% to 48%. At both the head (apse or east side) and foot (entrance or west side) of the north wall, relative humidity rose again in the autumn, with a mean value of 50% at mote 6 and 55% at mote 2. In this wall, relative humidity was observed to fluctuate more significantly in the summer than in the winter (Fig. 4). In the south wall, by contrast, at the foot of the church (mote 4), RH ranged from 45% to 60% in both winter and spring, while in the wall around the south entrance to the church (mote 7), spring and summer humidity fluctuated from 50% to 55% (Figs. 3 and 4). In late August, at the head of the church on the south (as on the north) façade, relative humidity (mote 7) declined steadily to values of around 30%, while tending to rise and vary more widely in the autumn, when the high values climbed to nearly 80% at the foot (mote 4) and 60% at the head (mote 7) of the church. The downward pattern exhibited greater fluctuations at the south foot of the church (mote 4). Relative humidity was 55–62% in winter and spring, although values of nearly 90% were recorded in mid-May. In the summer, the relative humidity readings at 240 cm in the apse tended to decline to minimum values of 35% (Figs. 3 and 4), rising in the autumn to 52% (Fig. 3).

The yearly rainy seasons affected church wall humidity. At Talamanca de Jarama, rainfall tends to be heaviest in April, October and November. In April 2012 it rained in the first half of the month, in October in the second half, and in November throughout, although more intensely in the first half. The indoor relative humidity in the church rose for several days in all three rainy periods. At 140 cm, no significant changes in humidity were recorded in the north wall, for the sensors were saturated at 100% before the rain. In the south wall, both around the apse and in the area near the entrance (mote 7), relative humidity was essentially flat, with a slight upward tendency. The greatest changes were observed at the foot of the church in that wall (mote 4), where RH rose from 93% to 96% after the rain on 24–26 October (Fig. 3).

4.2.2. Effect of temperature (solar radiation)

Building orientation in respect of solar radiation has a very direct impact on in-wall temperature: the sensors oriented southward recorded cyclic fluctuations (Fig. 5). The highest temperature was recorded by the south wall sensors (Fig. 6). In the apse area, which also faces south, the high temperature was considerably lower due primarily to the fact that the sensors were at a greater depth from the outside surface, even though summertime temperature fluctuations were detected.

Consequently, the differences recorded by the south-oriented sensors on the sunniest summer and winter days were chosen for characterisation and analysis. The warmest day was 26 June, six days after the summer solstice (20 June 2012). The solar elevation angle was 73 and the azimuth 244 ; the sun rose at 6:45 AM and 58 N and set at 9:49 PM and 302 N (Spanish official DST), for a 15-h, 4-min day. The cloud cover was scant on that day, although it intensified toward in the late afternoon, climbing to 90% by 2:00 PM on 27 June, after which it began to disappear. The sky was completely clear by 7:00 AM on 28 June and remained clear for the rest of the day. At the time of highest solar radiation on 26, 27 and 28 June, the wind was blowing from the SW at 3, 5 and 9 m/s, respectively. The outdoor temperature on the 26th was 41.6 C, 35.8 C on the 27th and 38 C on the 28th. These highs were recorded at 6:55 PM, except on the 27th, the only cloudy day, when the high was reached at 3:00 PM (Table 1). The minimum outdoor relative humidity values on those three days were 13%, 18% and 10%, respectively (Fig. 7a).

According to the iButton readings, temperatures were highest in the sensors positioned at 240 cm, where they ranged from 25.1 to 29.3 C on both the south and north walls on the three days in question. At 40 cm, the lowest level, the indoor temperature in the church was lower than in the upper areas, with values ranging from 23.6 to 26.7 C on 26, 27 and 28 June.

The sensors placed inside the south wall at motes 4 and 7 recorded daily solar radiation-induced fluctuations in temperature, but with a thermal lag with respect to the high outdoor temperature. On 26 June, the warmest day in the summer solstice timeframe, the highest outdoor temperature was reached at 6:55 PM,

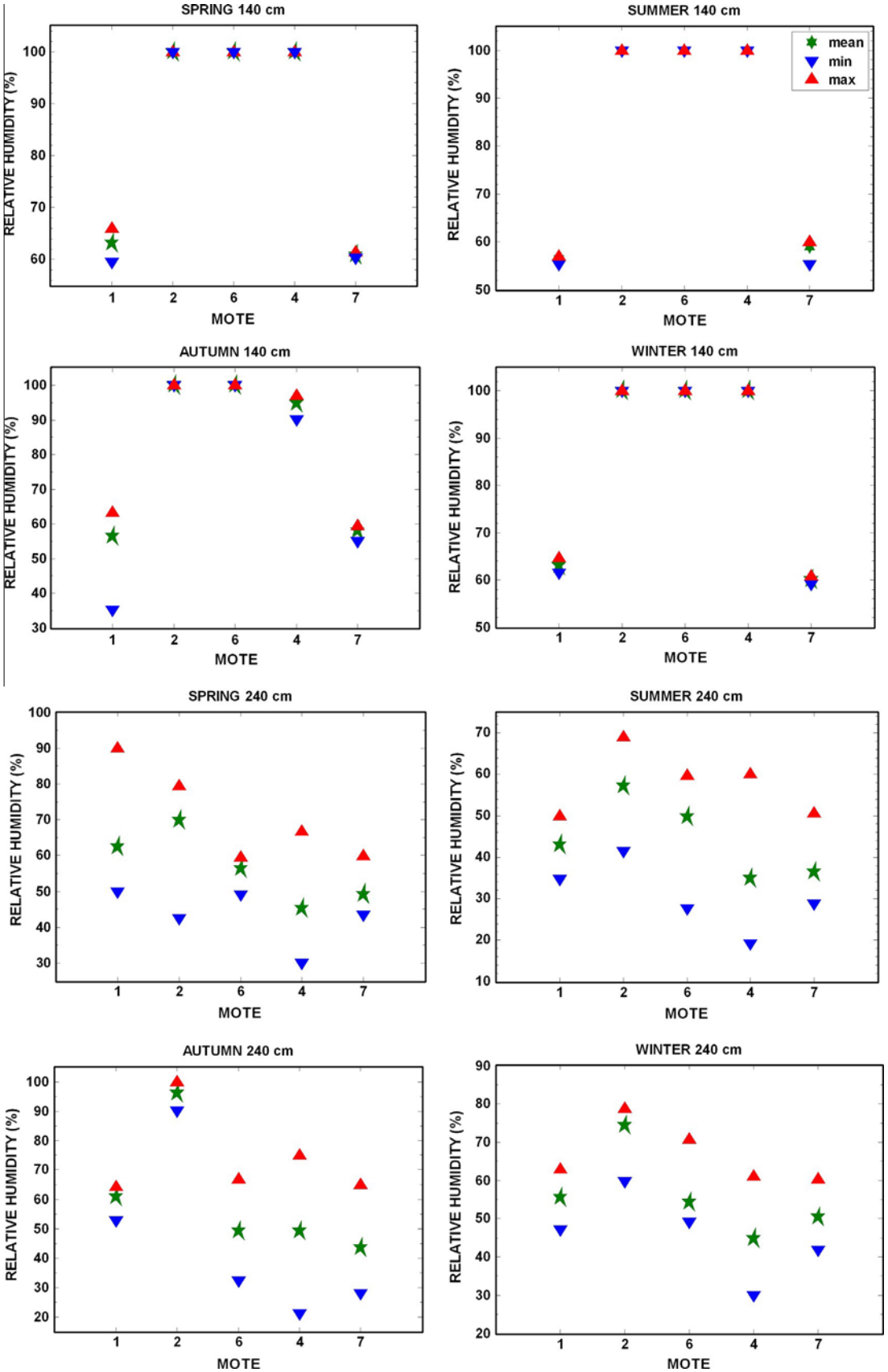

Fig. 3. Mean, high and low in-wall relative humidity values at 140 and 240 cm by season and mote: (1) apse, (2 and 6) north wall, (4 and 7) south wall.

whereas inside the church walls, the highest temperatures were recorded between 5:00 and 9:00 AM the next day, i.e., an 11–16-h lag, depending on sensor height. Fig. 7 shows the variations in the outdoor temperature and in the in-wall readings at different

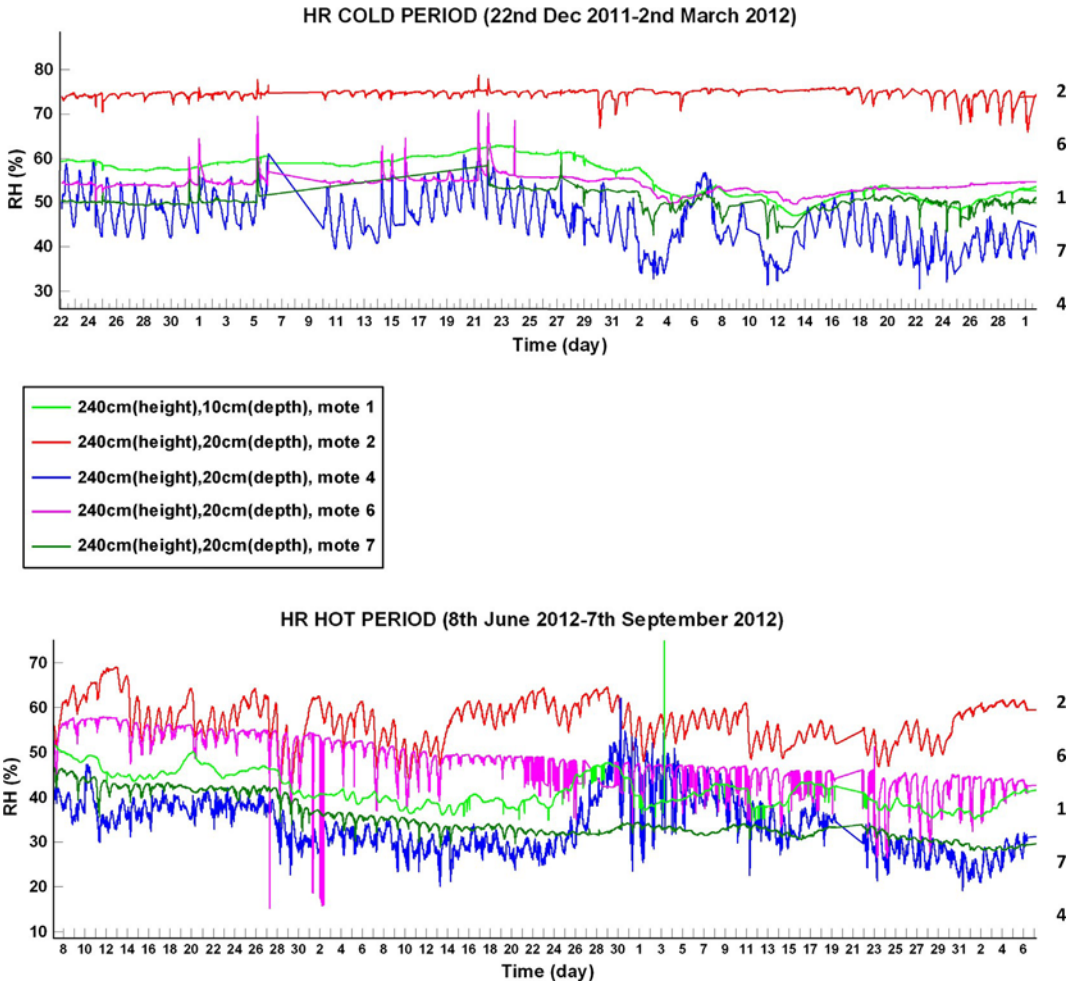

Fig. 4. (a) Variations in in-wall relative humidity for periods representative of cold autumn–winter conditions; (b) variations in in-wall relative humidity for periods representative of warm conditions.

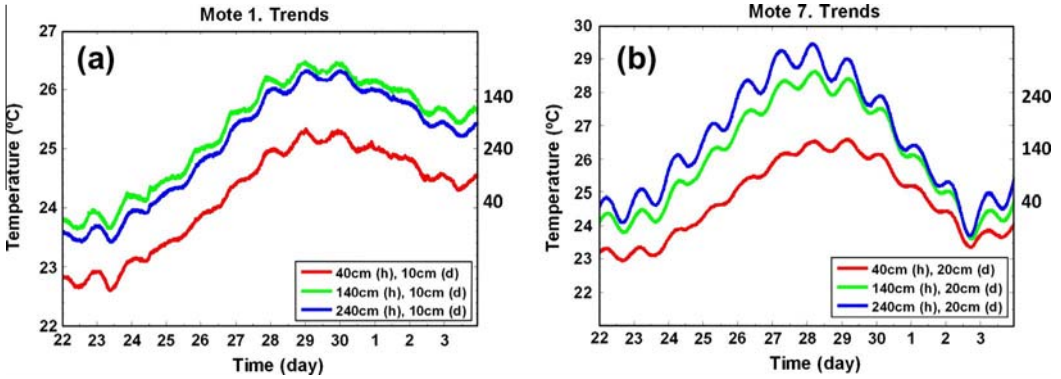

Fig. 5. Cyclic temperature behaviour around the summer solstice (22 June to 3 July 2012) (a) in the apse (mote 1, dolostone); (b) in the south-facing rubble masonry wall (mote 7).

heights on the south wall. Table 2 gives the thermal lag and differences between the high temperature recorded by the outdoor, indoor and embedded sensors. The highest in-wall temperatures, 30.5 and 29.3 C, were recorded at 240 cm by south-oriented motes 4 and 7, respectively. Temperature tended to decline with sensor height, with 40-cm readings of 28.4 and 26.2 C, respectively, at motes 4 and 7. The temperature inside the apse stone wall, which was lower than in the brick rubble masonry wall, was similar at 240 and 140 cm (25.4 and 25.6 C) and lower still (24.4 C) at 40 cm.

The difference between the outdoor and in-wall high temperatures tended to widen in the lower parts of the wall, where the lowest summertime temperatures were recorded and where the fluctuation at a given sensor was also narrower in the summer (Table 2).

In the apse area (mote 1), the highest temperature (24.4 C at 240 cm) was lower than on the south wall of the nave. While the apse stone temperature also varied at any given sensor, the fluctuation was slightly wider in the lower part of the wall: a 1- C difference was recorded at 40 cm compared to 0.6 C at 240 cm. The

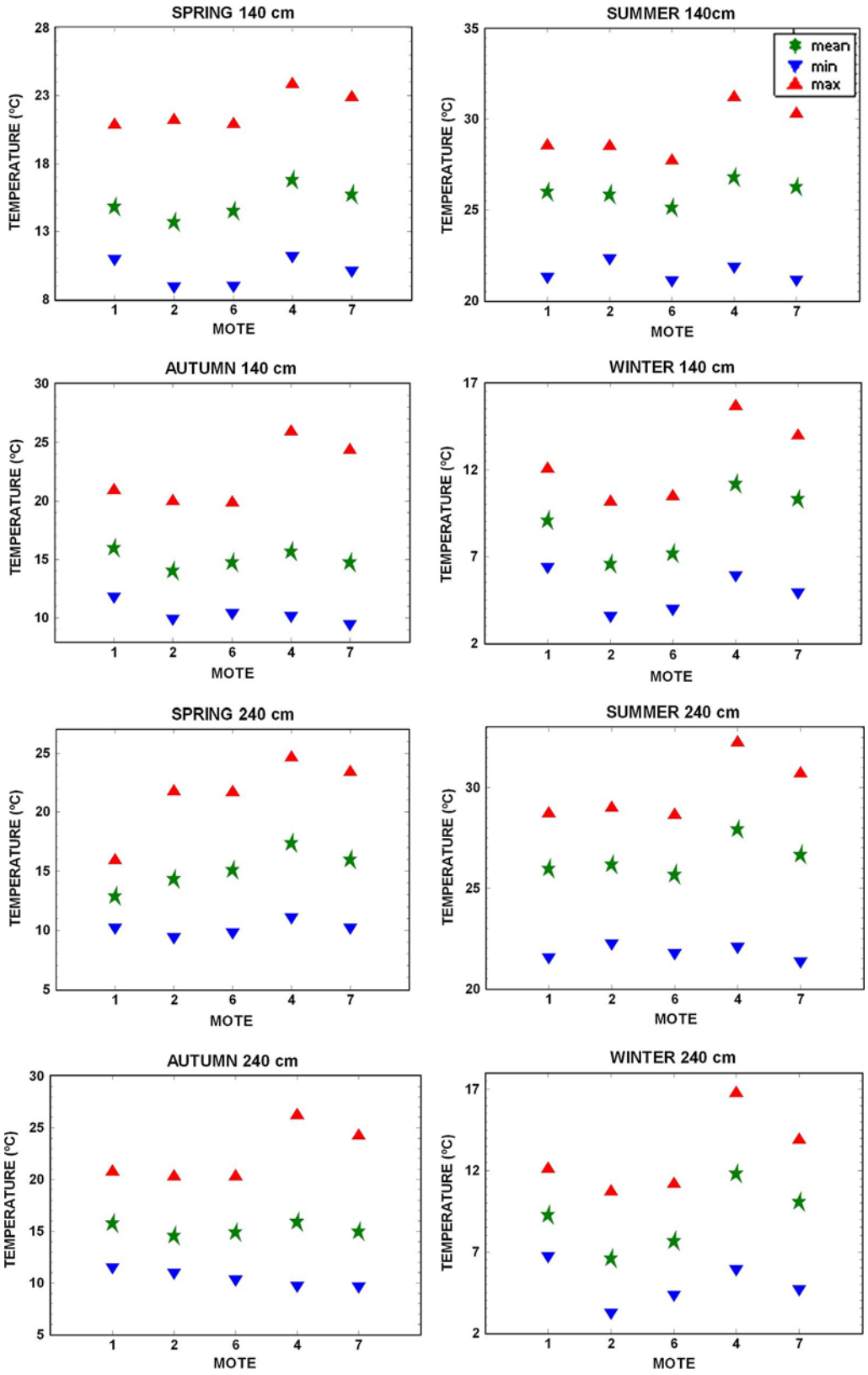

Fig. 6. Mean, high and low temperatures at 140 and 240 cm by season and mote: (1) apse, (2 and 6) north wall, (4 and 7) south wall.

thermal lag in the apse area was shorter than in the church nave. The lag values in the ashlar stone in the apse ranged from 5 to 2 h, compared to 11 to 16 h in the rubble masonry. The greatest lag was recorded in the lower part of the wall (Table 2). A similar pattern was observed on the following days, with 1- C temperature differences between the readings at 40 and 240 cm (Fig. 7b).

In winter, the highest solstice-related (21 December 2012) temperature was reached on 24 December, when it climbed to 11.3 C

Table 1
Outdoor weather conditions on 26 (the warmest day of the year), 27 and 28 June.

Date	T (C)		RH (%)	Wind	
	Max.	Time	Min	Direction	Speed (m/s)
26 June	41.6	6:55 PM	13	SW	3
27 June	35.8	3:00 PM	18	SW	5
28 June	38	6:55 PM	10	SW	7

at 4:44 PM. The wintertime temperature inside the wall was higher on the south façade, mote 4, than outdoors, whereas in the area around the south entrance (mote 7), where solar radiation was lower (Fig. 8). The thermal lag in the wall was shorter than in the summer, for the highest temperatures were reached at the foot of the church (mote 4) after 8.5 and 11.5 h, and after 11 h at mote 7. The temperature fluctuated more in the higher (1.7–0.9 C) than in the lower (1.0–0.5 C) parts of the wall and the

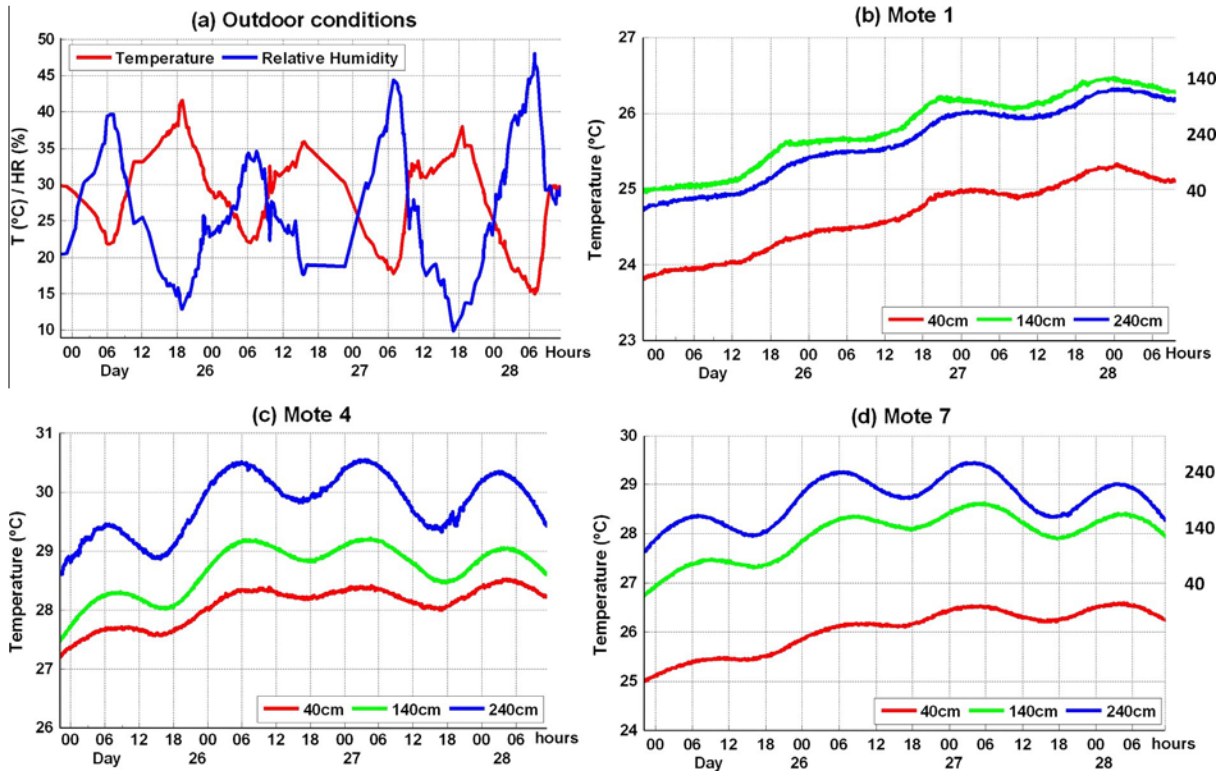

Fig. 7. Variations in outdoor temperature and in-wall south façade temperature, 26–28 June (a) outdoor temperature and relative humidity; (b) temperature inside the apse wall (mote 1); (c) temperature inside the south wall at mote 4; (d) temperature inside the south wall at mote 7.

Table 2
Thermal lag and temperature variations attributable to solar radiation: south wall, motes 1, 4 and 7.

Mote	Sensor	High T (C)	Change in T (C)	Daily T fluctuation (C)	Thermal lag (h)	Decrement Factor
26–27 June 2012						
	Outdoor	41.6	–	19.8	–	–
1	Indoor	27.4	14.2	2.0	0.4	0.10
	240 cm	25.4	16.2	0.6	4	0.03
	140 cm	25.6	16.0	0.6	2.2	0.03
	40 cm	24.4	17.2	1.0	4.9	0.05
4	Indoor	27.7	13.9	2.9	0.6	0.15
	240 cm	30.5	11.1	1.6	10.6	0.08
	140 cm	29.2	12.4	1.2	11.6	0.06
	40 cm	28.4	13.3	0.8	15.9	0.04
7	Indoor	28.4	13.2	2.4	0.9	0.12
	240 cm	29.3	12.3	1.3	10.7	0.07
	140 cm	28.3	13.3	1.4	12.7	0.07
	40 cm	26.2	15.5	1.1	13.0	0.06
24–25 December 2012						
	Outdoor	11.3	–	11.0	–	–
4	Indoor	11.1	0.2	0.3	0.1	0.0
	240 cm	13.0	1.7	1.5	8.5	0.13
	140 cm	12.1	0.8	1.0	10.8	0.09
	40 cm	12.5	1.2	0.5	11.4	0.05
7	Indoor	10.8	0.4	0.9	2.5	0.2
	240 cm	10.4	0.9	0.9	10.8	0.08
	140 cm	10.9	0.3	0.9	11.3	0.08
	40 cm	10.9	0.3	0.5	11.0	0.05

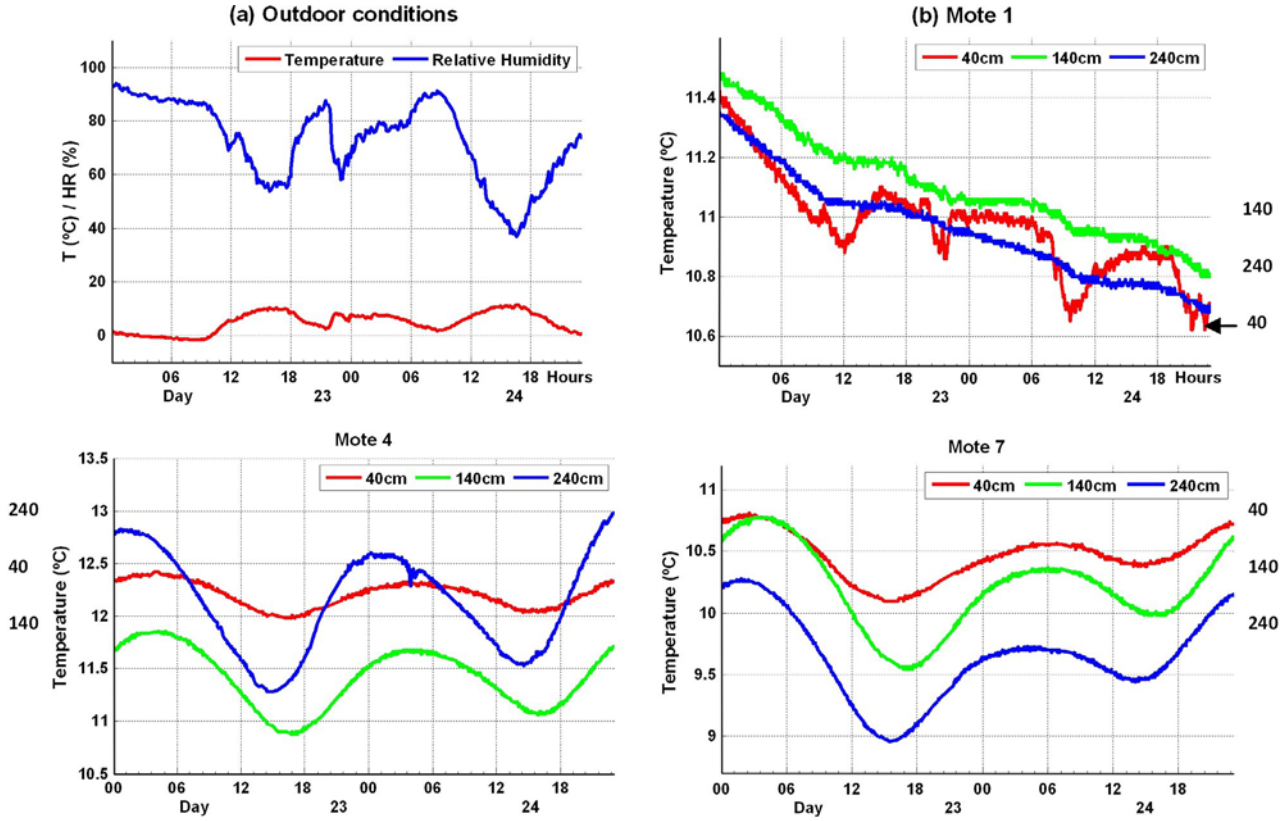

Fig. 8. Variations in outdoor temperature and in-wall south façade temperature, 23–24 December: (a) outdoor temperature and relative humidity; (b) temperature inside the apse wall (mote 1); (c) temperature inside the south wall at mote 4; (d) temperature inside the south wall at mote 7.

Table 3
Linear regression equations for solar radiation-induced temperature differences recorded in winter and summer at three heights by south wall motes 1, 4 and 7.

	40 cm	140 cm	240 cm
(a) Upward temperature pattern in summer			
Mote 1 Dolostone	163 10 ^{4} x + 22.3	175 10 ^{4} x + 23.3	180 10 ^{4} x + 23.1
Mote 4 Rubble masonry	206 10 ^{4} x + 25.1	260 10 ^{4} x + 24.7	283 l0 ^{4} x + 25.5
Mota7 Rubble masonry	220 l0 ^{4} x + 22.1	272 10 ^{4} x + 23.9	273 10 ^{4} x + 24.5
(b) Upward temperature patter n in winter			
Mote 1 Dolostone	30 10 ^{4} x+7.1	39 10 ^{4} x + 6.4	41 10 ^{4} + 6.8
Mote 4 Rubble masonry	110 10 ^{4} x + 8.2	173 l0 ^{4} x + 6.6	202 l0 ^{4} x + 6.9
Mota7 Rubble masonry	106 l0 ^{4} x + 7.2	158 10 ^{4} x + 5.9	159 10 ^{4} x + 5.8
(c) Downward temperature pattern in summer			
Mote 1 Dolostone	60 10 ^{4} x + 25.3	64 10 ^{4} x + 26.5	72 10 ^{4} x + 26.4
Mote 4 Rubble masonry	263 l0 ^{4} x + 26.7	317 10 ^{4} x + 29.4	391 10 ^{4} x + 30.6
Mota7 Rubble masonry	252 10 ^{4} x+ 26.9	379 10 ^{4} x + 28.9	397 10 ^{4} x + 29.4
(d) Downward temperature pattern in winter			
Mote 1 Dolostone	58 10 ^{4} x + 11.0	69 10 ^{4} x + 11.2	65 10 ^{4} x + 11.0
Mote 4 Rubble masonry	48 l0 ^{4} x + 12.2	52 10 ^{4} x + 11.4	53 10 ^{4} x + 12.1
Mota7 Rubble masonry	39 l0 ^{4} x + 10.4	47 l0 ^{4} x + 10.2	47 l0 ^{4} x + 9.6

difference between in-wall and outdoor temperature was much narrower than in the summer (Table 2). The lack of any significant variations in temperature in the apse in winter precluded thermal lag calculations in that part of the church.

Another significant factor is the trend in temperatures inside the walls immediately before and after the period of highest solar radiation, when the variations are most pronounced. Table 3 gives the linear regression equations for the temperature readings in the sensors embedded at the various heights in the south wall for different materials (dolostone, mote 1; rubble masonry, motes 4 and 7), when the outdoor temperature rose or declined over a period of approximately 15 days, in winter and summer. The summer solstice reference date was 26 June, when the highest temperature was recorded (Fig. 5). Of all the cycles exhibiting this type of variation throughout the year, this was the period when the steepest cumulative rise and decline in temperature were recorded.

Since no periods of significant wintertime rises or declines were observed during the year that temperatures were monitored, the slopes on the regression lines that defined upward and downward patterns were less accentuated than in the summer.

Moreover, the summertime variations between outdoor and in-wall temperature were narrower (on the order of 3 C) in the stone than in the rubble wall (6 C). The mote 4 and mote 7 findings for the rubble masonry showed very similar patterns and distributions.

Regression line lope increased with height in nearly all cases, although the difference between the readings for the two highest positions was sometimes slight (Table 3). The absolute value of the upward slope was greater in the rubble masonry (motes 4 and 7) than in the apse stone (mote 1). While in the summer the downward slope behaved in much the same way as the upward slope, in the winter the pattern reversed, with a steeper slope, i.e., a more intense decline in temperature, in the stone than in the rubble. Moreover, despite the slight increase in the slope with height, the 140- and 240-cm rubble masonry readings were similar and clearly distinguishable from the data for the lowest area of the wall. The slopes for the mote 1 (apse) regression lines were similar to one another, as were the slopes for the southward sensor readings (motes 4 and 7), where the similarity between the 140 and 240 cm sensor patterns was particularly visible.

An overall comparison of the slopes on the upward and downward regression lines showed that the upward slope for the summertime apse readings (mote 1) was three times greater than the downward slope, whereas the wintertime upward slope was 0.5 times the downward slope. In other words, the dolostone heated up more rapidly than it cooled in the summer, while the contrary was observed in the winter. This is consistent with the façade orientation.

In the rubble masonry (motes 4 and 7), the summertime upward slope was on the order of 0.8 times the downward slope: i.e., the southward rubble wall heated up more slowly than it cooled in this period. In the winter, the contrary was observed. Thermal differences were greater when the outdoor temperature rose than when it fell. The upward slope was on the order of twice the downward slope, meaning that in the winter the rubble walls heated up more rapidly than they cooled.

5. Discussion

Outdoor weather conditions impact the temperature and relative humidity inside the church. Indoor temperature tends to rise with the outdoor temperature, although the difference between the two values is on the order of 14 C. The thermal lag between the highest outdoor and highest indoor temperature was 0.4–0.9 h in the summer. In the winter thermal lag was somewhat greater in the area around the south entrance: 2.5 h. Such speedy thermal stabilisation was the result of church ventilation [30], for its two entrances as well as the door to the bell tower in the apse area are opened daily in the summer. Wintertime ventilation is less aggressive, for neither the door to the bell tower nor the south entrance is normally opened. The lag is consequently longer in that area.

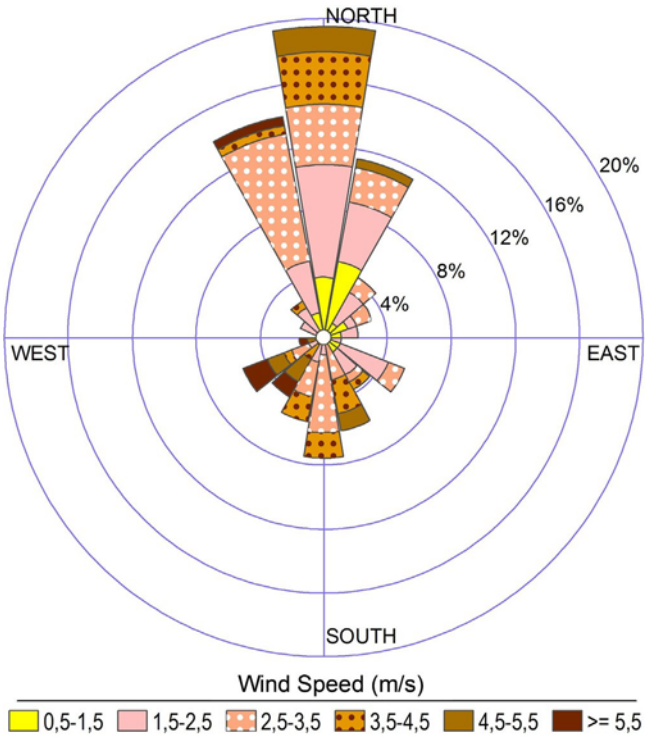

Fig. 9. Wind rose for rainy days in October–November 2012.

Much the same can be said about humidity. On rainy days the indoor relative humidity rises from around 45 to about 70–75%, where it remains for several days, only dropping to pre-precipitation values after around 48 h, although the time actually involved depends on cloud cover, temperature and outdoor relative humidity.

The walls of the church themselves are also affected by outdoor temperature and humidity. Solar radiation and rain are the two factors that induce the most substantial changes. The distribution of humidity inside the walls is indicative of capillary water absorption throughout the year, although water height tends to drop in late summer as a result of the lack of significant rainfall and the high outdoor temperatures in those months. As a result, the 40 cm high sensors were saturated throughout the year, as were the 140 cm instruments, whose humidity readings declined only in the summer and only on the south wall.

The rainy seasons raise in-wall humidity, a process favoured by gusts of wind [31,32]. Fig. 9 depicts the wind rose for rainy days in October and November. The façades are highly exposed, for on rainy days the wind was perpendicular to the north, and to a lesser extent, the south façade, albeit at low or moderate wind speed, which was not normally in excess of 5.5 m/s.

The humidity in the north wall may rise on rainy days, when the wind blows predominantly from the north, intensifying the impact on that side of the building [33]. Water absorption by the walls was only observed in the sensors positioned at 240 cm, the highest point, for the stone dado around the lower wall hinders water ingress. Nonetheless, rain may induce higher humidity in the stone and brick rubble by significantly affecting the sorptivity of these materials, which in turn generates humidity variations at 140 cm. Rain also favours the absorption of capillary water from the subsoil, which would explain why the lower parts of the wall are permanently saturated. Water is absorbed much more slowly across the apse wall, primarily because of its thickness. Moreover, stone hydraulic behaviour may differ substantially from the behaviour observed in the brick and clay fill in the nave walls.

In addition, while rain clearly impacts water ingress in the walls, the possible role of condensation on water absorption cannot be ruled out [34,35]. The highest in-wall humidity attributed to capillary absorption was found in the north wall, as well as in the south wall at the foot of the church.

The largest difference in temperature between the south and north walls is induced by solar radiation [2]. The materials used to build these walls have a specific heat (C) of 800 to 1000 J/kg K, but these values may climb to 1500 J/kg K when they are water-saturated, for the specific heat for water is 4186 J/kg K [15,36,37]. The south façade masonry can be divided into two clearly distinguishable parts: a 90-cm high rubble stone-clad brick dado and a brick and rubble stone checkerboard wall. The north wall, by contrast, consists primarily of rough limestone rubble with a clay and brick fragment fill. The apse is made of dolostone ashlars. These differences and the presence of moisture in the lower part of the walls determine variations in the heat capacity of the materials and solar heat transfer, both between walls and within each at different heights.

In the south-facing rubble wall, the thermal lag at a depth of 30 cm from the outer surface of the façade was from 10.6 to 11.6 h in the upper part of the wall, whereas in the lower area, consisting of a solid brick dado with a rubble stone cladding, the lag was longer, from 13 to 15 h. These values are similar to the findings reported by other authors [38]. In another vein, at around 0.1, the decrement factor [15,39,40], together with the thermal lag, enhance indoor comfort in the church [41].

Thermal lag is lower in the apse than in the nave wall, because while thermal conductivity ranges from 1.6 to 6.5 W/m K in dolostone [41,42], the respective values for solid brick and clay fill are 0.62 W/m K [13] and 1.9–2.0 W/m K [43].

The thermal diffusion of materials also rises with their moisture content and the presence of salt [44]. The areas at less than 40 cm from the floor therefore transfer heat more quickly because of their high salt content, attested to by the efflorescence visible on their surface.

The walls are water-saturated between 40 and 140 cm. With solar radiation-induced evaporation, the summertime temperature in the surrounding indoor and outdoor air declines. In the winter, when the outdoor temperature is lower, no evaporation takes place and the temperature rises. This explains why the heat curve for the lower areas of the south wall tends to raise the temperature more than the heat curve at 240 cm, inducing a thermal inversion. This is favoured by the fact that the impact of solar radiation may be more intense at a height of 40 cm, where it may be enhanced by the rise in the temperature of the outdoor pavement, leading to a steeper rise in temperature in the lower wall.

On the south wall, which receives solar radiation, heat absorption varied between mote 7 at the head and mote 4 at the foot of the church. This difference can be explained by the fact that while mote 7 benefitted from the shade afforded by the tower early in the morning and the roof over the main entrance portal in the afternoon, inasmuch as it was positioned between the two elements, mote 4 did not and was therefore exposed to greater solar radiation. While that shade affects the temperature transferred to the inside of the wall, it generates no change in the shape of the heat cycle (Fig. 7). The inference is that the damage caused by such temperature variations must be much greater on the outer surface than inside the wall, for they take place more quickly in the former [45].

6. Conclusions

The highest in-wall humidity attributed to capillary absorption was found in the north wall, as well as in the south wall at the foot of the church. San Juan Bautista Church construction affects water absorption by its walls and their response to solar radiation. The poorest quality construction is observed in the north wall, whose low rubble stone dado, surfaced on the inside with clay, exhibits higher sorptivity than the solid brick dados lined on the outside with fine or rough hewn dolostone ashlars on the south and west façades. Capillary water absorption is lowest in the apse, where the wall, made of dolostone ashlars, is thicker than in the rest of the church. The wind direction during the rainy seasons also tends to raise the humidity in the north wall.

These differences and the presence of moisture in the lower part of the walls determine variations in the heat capacity of the materials and solar heat transfer, both between walls and within each at different heights. Thermal lag is therefore longer in the lower part of the south wall, with its double layer of solid brick and dolostone rubble stone cladding, than in the upper areas, which consist of rubble masonry alone.

The north wall is at greatest risk of decay due to rain action and high moisture content, whereas the south façade is more exposed to solar radiation and daily wet/dry cycles, intensified by evaporation in the warmest seasons. The acceleration of decay attributable to shade is not significant inside the wall, where no thermal variations were recorded.

Wall thermal lag and decrement factor values contribute to indoor comfort in the church by transferring the heat absorbed during the day. Moreover, further to the upward and downward regression lines, greater comfort is afforded by rubble stone than ashlar constructions.

Acknowledgements

The cooperation received from the Laboratory Network in Science and Technology for Heritage Conservation (RedLabPat, CEI Moncloa) and the Diocese of Alcalá is gratefully acknowledged. The present study was funded under projects CGL2011-27902, BIA2009-14395-C04-01, GEOMATERIALES (S2009/MAT-1629), CONSOLIDER-TCP (CSD2007-0058). M.I. Martínez-Garrido's participation was supported by a Moncloa Campus of International Excellence (UPM-UCM, CSIC) PICATA predoctoral fellowship. Dr. S. Aparicio worked under the Spanish National Research Council's Post Graduate Studies Council post-doctoral program. The manuscript was edited by Margaret Clark, professional translator and English language science editor.

References

[1] Simonson CJ, Salonvaara M, Ojanen T. The effect of structures on indoor humidity – possibility to improve comfort and perceived air quality. Indoor Air 2002;12:243–51.
[2] Tavil A. Thermal behavior of mansory walls in Istanbul. Constr Build Mater 2004;18(2):111–8.
[3] Orosa JA, Baaliña A. Improving PAQ and comfort conditions in Spanish office buildings with passive climate control. Build Environ 2009;44:502–8.
[4] Sandrolini F, Franzoni E, Sassoni E, Diotallevi PP. The contribution of urban-scale environmental monitoring to materials diagnostics: a study on the Cathedral of Modena (Italy). J Cult Heritage 2011;12(4):441–50.
[5] Gómez-Heras M, Fort R. Location of quarries of non-traditional stony materials in the architecture of Madrid: The crypt of the Cathedral of Santa María la Real de la Almudena. Mater Constru 2004;54:33–49.
[6] Camuffo D. Indoor dynamic climatology: investigations on the interactions between walls and indoor environment. Atmos Environ 1983;17(9):1803–9.
[7] Espinosa RM, Franke L, Deckelmann G. Phase changes of salts in porous materials: crystallization, hydration and deliquescence. Constr Build Mater 2008;22(8):1758–73.
[8] Grossi CM, Brimblecombe P, Menéndez B, Benavente D, Harris I, Déqué Espinosa M, et al. Sci Total Environ 2011;409:2577–85.
[9] Viitanen H, Vinha J, Salminen K, Peuhkuri R, Paajanen L, Lahdesmaki K, et al. J Build Phys 2010;33,3:201–24.
[10] Kazuhide I. Numerical prediction model for fungal growth coupled with hygrothermal transfer in building materials. Indoor Built Environ 2012;21(6):845–56.
[11] López-Arce P, Fort R, Gómez-Heras M, Perez-Monserrat E, Varas MJ. Preservation strategies for avoidance of salt crystallisation in El Paular Monastery cloister, Madrid Spain. Environ Earth Sci 2010;63:1487–509.
[12] Ignatavicius C, Ignatavicius G. Investigation of damage and microclimate deterioration caused by dampness in the palace of signatories to the declaration of independence. Indoor Built Environ 2005;14(1):89–95.
[13] Torres I, Peixoto de Freitas V. The influence of the thickness of the walls and their properties on the treatment of rising damp in historic buildings. Constr Build Mater 2010;24:1331–9.
[14] Aste N, Angelotti A, Buzzetti M. The influence of the external walls thermal inertia on the energy performance of well insulated buildings. Energy Build 2009;41:1181–7.
[15] Asan H, Sancaktar YS. Effects of Wall's thermophysical properties on time lag and decrement factor. Energy Build 1998;28:159–66.
[16] Budaiwi I, El-Diasty R, Abdou A. Modelling of moisture and thermal transient behaviour of multi-layer non-cavity walls. Build Environ 1999;34(5):537–51.
[17] Kontoleon KJ, Eumorfopoulou EA. The influence of wall orientation and exterior surface solar absorptivity on time lag and decrement factor in the Greek region. Renew Energy 2008;33(7):1652–64.
[18] Moradias PA, Silva PD, Castro-Gomes JP, Salazar MV, Pires L. Experimental study on hygrothermal behaviour of retrofit solutions applied to old building walls. Constr Build Mater 2012;35:864–73.
[19] Lankester P, Brimblecombe P. The impact of future climate on historic interiors. Sci Total Environ 2012;417–418:248–54.
[20] de Wilde P, Tian W. Management of thermal performance risks in buildings subject to climate change. Build Environ 2012;55:166–77.

[21] Brunet M, Jesús Casado M, de Castro M, Galán P, López JA, Martín JM, Pastor A, Petisco E, Ramos P, Ribalaygua J, Rodríguez E, Sanz I, Torres L. Generación de escenarios regionalizados de cambio climático para España. Ministerio de medio ambiente, medio rural y marino. Gobierno de España 2009; 158 p.

[22] Saïd MNA, Brown WC, Shirtliffe CJ, Maurenbrecher AHP. Monitoring of the building envelope of a heritage house: a case study. Energy Build 1999;30:211–9.

[23] Martínez-Garrido, MI, Aparicio S, Fort R, Izquierdo MAG, Anaya JJ. Risk of decay detected through wireless sensor networks. Science and Technology for the Conservation of Cultural Heritage, In: Rogerio-Candelera MA, Lazzari M, Canoy E, editors. CRC Press; 2013. ISBN: 978-1-13800-009-4.

[24] Mazzoli-Guintard, Christine. Petite ville de l'Islam medieval (IXe-XXIe siècles). Madrid: Presses Universitaires de Rennes; 2009. 268 pp.

[25] Fort R, Varas MJ, Alvarez de Buergo M, Freire DM. Determination of anisotropy to enhance the durability of natural stone. J Geophys Eng 2011;8:132–44.

[26] Fort R, Fernández-Revuelta B, Varas MJ, Álvarez de Buergo M, Taborda M. Effect of anisotropy on Madrid-region cretaceous dolostone durability in salt crystallization processes. Mater Constr 2008;58,289-290:161–77.

[27] Wightman P, Jimeno M, Jabba D, Labrador M, Zurbarán M, Córdoba C, et al. Empirical approach to network sizing for connectivity in wireless Sensor networks with realistic radio propagation models. Ad-hoc Mobile Wireless Networks 2011;6811:72–85.

[28] Aparicio S, Martínez-Garrido MI, Ranz J, Fort R, Izquierdo MAG, Anaya JJ. A Performance of tree and mesh routing topologies of wireless Sensor. Ad Hoc Networks. Unpublished results.

[29] Martínez-Garrido MI, Aparicio S, Fort R, Izquierdo MAG, Anaya JJ. Wireless sensor networking to asses the risk of decay in the built heritage, Ad Hoc & Sensor Wireless Networks. Unpublished results.

[30] Kalamees T, Korpi M, Vinha J, Kurnitsk J. The effects of ventilation systems and building fabric on the stability of indoor temperature and humidity in finnish detached houses. Build Environ 2009;44:1643–50.

[31] Pérez-Bella JM, Domínguez-Hernández J, Rodríguez-Soria B, del Coz-Díaz JJ, Cano-Suñén E. Estimation of the exposure of buildings to driving rain in Spain from daily wind and rain data. Build Environ 2012;57:259–70.

[32] Guardia JJ, Varas MJ, Suárez FJ. Castle palace of La Calahorra, Granada: Influence of climatic and architectural factors in differential deterioration of their stone factories. Mater Constr 2012. http://dx.doi.org/10.3989/mc.2013.04112 [Online] Accepted manuscript.

[33] Abuku M, Janssen H, Roels S. Impact of wind-driven rain on historic brick wall buildings in a moderately cold and humid climate: numerical analyses of mould growth risk, indoor climate and energy consumption. Energy Build 2009;41:101–10.

[34] Camuffo D. Microclimate for cultural heritage. Developments in atmospheric science 23. Amsterdam: Elsevier; 1998.

[35] Krüger M, Samuels JM, Bachmaier SA, Lehmann F, Willeke J. Condensation risk analysis and indoor climate manipulation assisted by continuous monitoring at Johanniskirche in Schwäbisch Gmünd. In: M. Krüger, editor. Cultural heritage preservation – EWCHP 2011, Proc. of the European workshop on cultural heritage preservation. Berlin: Fraunhofer IRB Verlag; 2011.

[36] Baggs D, Mortensen N. Thermal mass in building design BDP environment design guide. Royal Aust Inst Architects 2006;4:1–8.

[37] Meukam P, Jannot Y, Noumowe A, Kofane TC. Thermo physical characteristics of economical building materials. Constr Build Mater 2004;18(6):437–43.

[38] Jin X, Zhang X, Cao Y, Wang G. Thermal performance evaluation of the wall using heat flux time lag and decrement factor. Energy Build 2012;47:369–74.

[39] Ulgen K. Experimental and theoretical investigation of effects of Wall's thermophysical properties on time lag and decrement factor. Energy Build 2002;34:273–8.

[40] Flores Larsen S, Filippí C, Lesino G. Thermal behavior of building walls in summer: comparison of available analytical methods and experimental results for a case study. Build Simul 2009;2:3–18.

[41] Taylor P, Luther MB. Evaluating rammed earth walls: a case study. Solar Energy 2004;76(1–3):79–84.

[42] Kobranova VN. Petrophysics. Mir Publishers; 1989.

[43] Minke G. Earth construction handbook. The building material earth in morden architecture. Southampton (UK): WIT Press; 2000. 206 p.

[44] Tikhonravova PI. Effect of the water content on the thermal diffusivity of clay loams with different degrees of salinization in the Transvolga region Eurasian. Soil Sci 2007;40(1):47–50.

[45] Gómez-Heras M, Smith BJ, Fort R. Influence of surface heterogeneities of building granite on its thermal response and its potential for the generation of thermoclasty. Environ Geology 2008;56(3–4):547–60.